Petroleum Science 21 (2024) 1765–1779

Contents lists available at ScienceDirect

Petroleum Science

journal homepage: www.keaipublishing.com/en/journals/petroleum-science

Original Paper

Study of the pressure transient behavior of directional wells considering the effect of non-uniform flux distribution

Yan-Zhong Liang , Bai-Lu Teng , Wan-Jing Luo *

School of Energy Resources, China University of Geosciences (Beijing), Beijing, 100083, China

ARTICLE INFO

Article history:
Received 3 May 2023
Received in revised form
13 December 2023
Accepted 18 December 2023
Available online 28 December 2023

Edited by Yan-Hua Sun and Meng-Jiao Zhou

Keywords:
Directional well
Pressure transient behavior
Semi-analytical model
Non-uniform flux

ABSTRACT

During the production, the fluid in the vicinity of the directional well enters the wellbore with different rates, leading to non-uniform flux distribution along the directional well. However, in all existing studies, it is oversimplified to a uniform flux distribution, which can result in inaccurate results for field applications. Therefore, this paper proposes a semi-analytical model of a directional well based on the assumption of non-uniform flux distribution. Specifically, the direction well is discretized into a carefully chosen series of linear sources, such that the complex well trajectory can be captured and the non-uniform flux distribution along the wellbore can be considered to model the three-dimensional flow behavior. By using the finite difference method, we can obtain the numerical solutions of the transient flow within the wellbore. With the aid of Green's function method, we can obtain the analytical solutions of the transient flow from the matrix to the wellbore. The complete flow behavior of a directional well is perfectly represented by coupling the above two types of transient flow. Subsequently, on the basis of the proposed model, we conduct a comprehensive analysis of the pressure transient behavior of a directional well. The computation results show that the flux variation along the direction well has a significant effect on pressure responses. In addition, the directional well in an infinite reservoir may exhibit the following flow regimes: wellbore afterflow, transition flow, inclined radial flow, elliptical flow, horizontal linear flow, and horizontal radial flow. The horizontal linear flow can be observed only if the formation thickness is much smaller than the well length. Furthermore, a dip region that appears on the pressure derivative curve indicates the three-dimensional flow behavior near the wellbore.

1. Introduction

Directional wells have been widely applied in petroleum exploration and development to improve production performance (Guan et al., 2021). Particularly in developing offshore reservoirs, directional wells can significantly reduce the required number of platforms compared to vertical wells (Islam and Hossain, 2021). Pressure transient analysis is a powerful tool to forecast well performance and evaluate reservoir properties (Zarrouk and Mclean, 2019). In field applications, studying the pressure transient of directional wells can provide theoretical instruction for optimizing production systems. Three types of methods have been widely used for conducting pressure transient analysis, including numerical method, analytical method, and semi-analytical method. Among these three types of methods, the numerical method is greatly effective for describing the transient flow behavior of complex well types (Gill et al., 2007). However, the numerical method is normally more computationally demanding and inconvenient because it requires numerous discrete grids to model three-dimensional flow behaviors. Moreover, various analytical methods have been developed to conduct the pressure transient analysis on different well types (Fair et al., 1999; Ozkan and Raghavan, 2000; Bond et al., 2006). Cinco et al. (1975) first used the instantaneous source function to study the pressure response of directional wells with a uniform flux distribution. Ozkan et al. (1999) presented a 3D analytical model to simulate the transient pressure behavior of slant and horizontal wells. Sousa and Moreno (2015) presented a new study of the directional well with a uniform flow condition using Green's function and superposition principle. Feng and Liu (2015) studied the wellbore pressure dynamics of slant wells by using the mirror image principle on the basis of the point source solution. Miranda et al. (2016) provided a uniform-flux solution of the restricted-entry well in anisotropic reservoirs based on Green's

* Corresponding author.
E-mail address: luowanjing@cugb.edu.cn (W.-J. Luo).

https://doi.org/10.1016/j.petsci.2023.12.014

Nomenclature

a, b, c, A	Parameters defined in Appendix A
$\boldsymbol{A}$, $\boldsymbol{B}_1$, $\boldsymbol{B}_2$, $\boldsymbol{C}$, $\boldsymbol{D}$, $\boldsymbol{G}$, $\boldsymbol{p}_w$, $\boldsymbol{q}^n$	Matrices defined in Appendices A and B
A_w	The area of the wellbore cross-section
B	Formation volume factor, m^3/m^3
c_{tm}	Matrix total compressibility, MPa^{-1}
c_{tw}	Wellbore total compressibility, MPa^{-1}
c_s	Dimensionless coefficient defined in this work
C_w	Wellbore storage coefficient, bbl/psi
C_{wD}	Dimensionless wellbore storage coefficient
h	Formation thickness, m
h_D	Dimensionless formation thickness
k_m	Matrix permeability, mD
k_w	Wellbore permeability, mD
k_D	Dimensionless wellbore permeability
l	Space position along the inclined direction of the well, m
l_i	Space position along the inclined direction of the well panel (i), m
l_D	Dimensionless space position along the inclined direction of the well
L	Well total length along the inclined direction, m
Δl	Wellbore-element length along the inclined direction, m
Δl_D	Dimensionless wellbore element's length along the inclined direction
N_w	Number of elements of the discretized well
p	Pressure, MPa
p_i	Initial reservoir pressure, MPa
p_w	Wellbore pressure, MPa
p_{wD}	Dimensionless wellbore pressure
p_{wb}	Bottomhole pressure, MPa
p_{wbD}	Dimensionless bottomhole pressure
q	Flux rate from the matrix to the wellbore under standard conditions, m^3/d
q_D	Dimensionless flux
q_w	Well production rate under standard conditions, m^3/d
$q_{w\text{-}wb}$	Flux rate from the heel of the directional well into the vertical wellbore under the standard condition, m^3/d
$q_{w\text{-}wbD}$	Dimensionless flux rate from the heel of the directional well into the vertical wellbore
r_w	Wellbore radius, m
r_{wD}	Dimensionless wellbore radius
t	Time, d
t_D	Dimensionless time
x, y and z	x-, y- and z-coordinates, m
x_D, y_D, z_D	Dimensionless coordinate
x_0, y_0, z_0	Center position coordinates of the linear source, m
x_{0D}, y_{0D}, z_{0D}	Dimensionless center position coordinates of the linear source
z_e	Reservoir dimension, m
z_{eD}	Dimensionless reservoir dimension
z_w	Distance between the center of the directional well and the upper reservoir boundary, m
z_{wD}	Dimensionless distance between the center of the directional well and the upper reservoir boundary
$x(l_i)$, $z(l_i)$	Coordinates at position l_i, m
α	Diffusivity coefficient, m^2/d
β	Unit conversion factor that is equal to 0.0853
γ	Dimensionless coefficient
δ	The instantaneous flux
θ	Inclined angle, °
μ	Oil viscosity, mPa s
ϕ_m	Matrix porosity
ϕ_f	Effective porosity in the wellbore system

Subscript and superscript

i	Initial condition
m	Matrix
t	Total
w	Wellbore

function. Xu et al. (2021) developed an analytical model of the inclined well in a triple-porosity carbonate gas reservoir based on Laplace transform and pressure drop superposition. Shi et al. (2023) established a novel analytical solution to characterize the transient pressure behavior of horizontal wells in the multibranched fault-karst reservoir. From these studies, we have a preliminary understanding of the pressure transient behavior of directional wells. It is worth noting that, although the analytical solution has been used to study the pressure response of the directional wells in various complex field conditions. However, the effect of flux variation cannot be accounted for in their articles because of the pro-assumption, which will lead to errors with the actual situation.

In addition to the numerical method and the analytical method, numerous scholars have proposed various semi-analytical methods to characterize complicated flow behaviors (Khatteb et al., 1991; Wang et al., 2020; Albattat et al., 2022). Ezulike and Igbokoyi (2012) studied the pressure transient behavior of horizontal wells in anisotropic composite reservoirs and conducted a sensitivity analysis about the influence of key reservoir parameters on the pressure drop responses. Simonov et al. (2017) developed a semi-analytical model for describing the transient flow behavior of a multilateral well and considered the effects of finite conductivity fractures and friction losses. Luo et al. (2018) presented a semi-analytical model to research the productivity index of horizontal wells and obtained the distribution of dimensionless productivity index along the horizontal well. Teng and Li (2019) introduced a semi-analytical model to study the pressure transient behavior of the partially-penetrating inclined fracture and thoroughly researched the effect of flux variation with different fracture conductivities. Al-Kabbawi (2022) established an optimal semi-analytical model of the horizontal well with infinite conductivity. In this work, the instantaneous uniform-flux segmentary source function was used instead of the pressure superposition. Currently, it can be recognized that the semi-analytical method not only can consider the effect of flux variation but is more convenient than traditional numerical methods. This is because the semi-analytical method only requires discretization along the wellbore, without the need to discrete the entire reservoir. However, there is a lack of literature that can provide a semi-analytical model for describing the transient flow behavior of a directional well that would take into account the existence of flux variation along the wellbore.

In this paper, we conduct a comprehensive analysis of the pressure responses of a directional well that has a non-uniform flux distribution. With the aid of the semi-analytical method, the directional well is discretized into a certain number of segments to account for the complex well trajectories and the non-uniform flux variations. For each segment, the behavior of flow rate and pressure over time can be monitored. The validity of the method is

demonstrated by comparing it with results generated numerically by Eclipse. Subsequently, we apply the proposed model to depict the flux distribution along the wellbore at different wellbore parameters and successfully distinguish the main flow regimes from the computational results. In addition, we carry out the sensitivity analysis to clarify the influences of wellbore storage, wellbore radius, inclined angle, well vertical position, and formation thickness on the pressure dynamics.

2. Methodology

This work studies the pressure transient behavior of a directional well that produces single-phase oil from a single-layer reservoir. The schematic of the directional well and the reservoir are shown in Fig. 1. The upper and lower boundaries of the reservoir are impermeable, and the reservoir extends indefinitely in the horizontal direction. The assumptions employed to derive a semi-analytic model are listed as follows:

- The fluid and rock properties in the reservoir are assumed to be homogeneous and isotropic;
- The reservoir is bounded with impermeable upper and lower boundaries along the vertical direction and boundless along the horizontal direction;
- The vertical projection of the directional well is parallel to the *x*-axis;
- The flux variation along the wellbore is considered;
- The reservoir contains only single-phase oil;
- The equivalent wellbore permeability is obtained with the Poiseuille formula;
- The oil is produced with a constant rate;
- The gravity effect within the wellbore and wellbore storage are taken into account in the model;
- The temperature variation in the reservoir is neglected.

2.1. Definition of the dimensionless parameters

For the convenience of analysis and discussion, we define the following dimensionless variables:

$$p_D = \frac{2\pi\beta k_m h(p_i - p)}{q_w B\mu}, \quad p_{wD} = \frac{2\pi\beta k_m h(p_i - p_w)}{q_w B\mu} \tag{1}$$

$$t_D = \frac{\beta k_m t}{\phi_m \mu c_{tm} L^2} \tag{2}$$

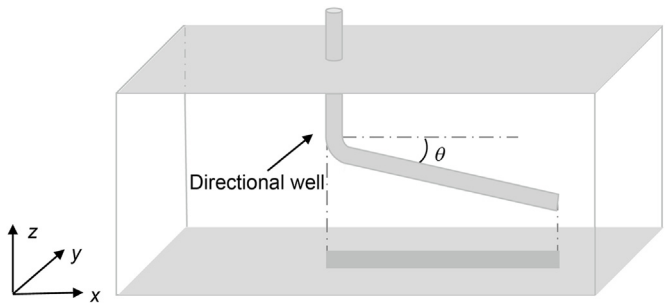

Fig. 1. Physical model of the directional well in a single-layer reservoir.

$$q_D = \frac{q}{q_w}, \quad q_{w\text{-}wbD} = \frac{q_{w\text{-}wb}}{q_w} \tag{3}$$

$$x_D = \frac{x}{L}, \quad y_D = \frac{y}{L}, \quad z_{eD} = \frac{z_e}{L}, \quad l_D = \frac{l}{L} \tag{4}$$

$$h_D = \frac{h}{L}, \quad r_{wD} = \frac{r_w}{L} \tag{5}$$

$$\gamma = \frac{0.0434 B r_w^2}{L^2}, \quad C_{wD} = \frac{C_w}{2\pi h \phi_m c_{tm} r_w^2} \tag{6}$$

$$C_s = \frac{\phi_w c_{tw}}{\phi_m c_{tm}}, \quad k_D = \frac{k_w}{k_m} \tag{7}$$

2.2. Numerical formulation of the directional well system

As shown in Fig. 2, we discrete the directional well into N_w elements in the proposed model to capture its trajectory, and these elements have the same dimension. In this figure, Δl is the length of the discrete element along the inclined direction, and A_w is the area of the wellbore cross-section. The cross-section of the wellbore is much smaller than the length of the well, therefore the flow of fluid in the wellbore can be simplified to one-dimensional flow. The transient flow equation of a directional well can be expressed as (Ertekin et al., 2001)

$$\frac{\partial^2 p_w}{\partial l^2} + \frac{B\mu q}{\beta \Delta l A k_w} = \frac{\mu \phi_w c_{tw}}{\beta k_w} \frac{\partial p_w}{\partial t} \tag{8}$$

Eq. (8) is derived from the mass balance equation. Inserting Eqs. (1)–(7) into Eq. (8) and rewriting Eq. (8) into finite difference format gives

$$\left(\frac{1}{\Delta l_D^2} + \frac{C_s}{k_D}\frac{1}{\Delta t_D}\right) p_{D_i}^n - \frac{1}{\Delta l_D^2} p_{D_{i-1}}^n - \frac{1}{\Delta l_D^2} p_{D_{i+1}}^n + \frac{2h_D}{k_D \Delta l_D r_{wD}^2} q_{D_i}^n = \frac{C_s}{k_D}\frac{1}{\Delta t_D} p_{D_i}^{n-1} \tag{9}$$

Applying Eq. (9) to the N_w linear sources and arranging these N_w finite difference equations into a matrix format yield

$$\boldsymbol{A} \cdot \boldsymbol{p}_w^n + \boldsymbol{B}_1 \odot \boldsymbol{q}^n - \boldsymbol{B}_2 \odot q_{w\text{-}wD}^n = \boldsymbol{C} \odot \boldsymbol{p}_w^{n-1} \tag{10}$$

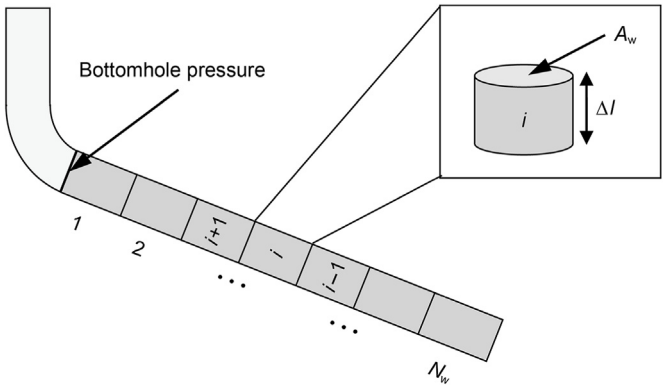

Fig. 2. Schematic of the directional well discretization along the inclined direction.

where ⊙ is the Hadamard product operator; $q_{\text{w-wD}}$ is dimensionless flux from the heel of the directional well into the vertical wellbore; and the matrices of $\boldsymbol{A}$, $\boldsymbol{p}_{\text{w}}$, $\boldsymbol{B}_1$, $\boldsymbol{q}^n$, $\boldsymbol{B}_2$, and $\boldsymbol{C}$ are defined in Appendix A.

2.3. Analytical solution of the matrix system

As aforementioned, the directional well is discretized into N_{w} elements, each of which can be considered a linear source. The pressure response that is induced by a single continuous linear source can be expressed as

$$p_{\text{i}} - p(x,y,z,t^n) = \frac{B}{\phi_{\text{m}} c_{\text{tm}} \Delta l} \frac{1}{z_{\text{e}}} \sum_{k=1}^{n} q^k \int_{t^{k-1}}^{t^k} \left\{ \exp\left[-\frac{(y-y_0)^2}{4\alpha(t^n-\tau)} \right] \Big/ \sqrt{4\pi\alpha(t^n-\tau)} \right\} \cdot \int_{l_i=0}^{l_i=\Delta l} \left\{ \exp\left[-\frac{(x-x_0(l_i))^2}{4\alpha(t^n-\tau)} \right] \Big/ \sqrt{4\pi\alpha(t^n-\tau)} \right\} \cdot \left\{ 1 + 2\sum_{m=1}^{\infty} \exp\left[-\frac{m^2\pi^2\alpha(t^n-\tau)}{z_{\text{e}}^2} \right] \cos\frac{m\pi z}{z_{\text{e}}} \cos\frac{m\pi z_0(l_i)}{z_{\text{e}}} \right\} \mathrm{d}l_i \mathrm{d}\tau \tag{11}$$

where x, y, and z are the spatial coordinates of the desired pressure response, and x_0, y_0, z_0 are the spatial coordinates of the central position of the linear source. Since the pressure response at an arbitrary position is influenced by all the N_{w} linear sources, according to the superposition principle, the total pressure change at position (x, y, z) can be obtained by summing up the pressure change induced by all the linear sources, which yields

$$p_{\text{i}} - p(x,y,z,t^n) = \frac{B}{\phi_{\text{m}} c_{\text{tm}} \Delta l} \frac{1}{z_{\text{e}}} \sum_{i=1}^{N_{\text{w}}} \sum_{k=1}^{n} q_i^k \int_{t^{k-1}}^{t^k} \left\{ \exp\left[-\frac{(y-y_{0i})^2}{4\alpha(t^n-\tau)} \right] \Big/ \sqrt{4\pi\alpha(t^n-\tau)} \right\} \cdot \int_{l_i=0}^{l_i=\Delta l} \left\{ \exp\left[-\frac{(x-x_0(l_i))^2}{4\alpha(t^n-\tau)} \right] \Big/ \sqrt{4\pi\alpha(t^n-\tau)} \right\} \cdot \left\{ 1 + 2\sum_{m=1}^{\infty} \exp\left[-\frac{m^2\pi^2\alpha(t^n-\tau)}{z_{\text{e}}^2} \right] \cos\frac{m\pi z}{z_{\text{e}}} \cos\frac{m\pi z_0(l_i)}{z_{\text{e}}} \right\} \mathrm{d}l_i \mathrm{d}\tau \tag{12}$$

Inserting the dimensionless coefficients in Eqs. (1)–(7) into Eq. (12), Eq. (12) can be rewritten as

$$p_{\text{wD}}(x_{\text{D}},y_{\text{D}},z_{\text{D}},t_{\text{D}}^n) = \frac{h_{\text{D}}}{2\Delta l_{\text{D}}} \frac{1}{z_{\text{eD}}} \sum_{i=1}^{N_{\text{w}}} \sum_{k=1}^{n} q_{\text{D}i}^k \int_{t_{\text{D}}^{k-1}}^{t_{\text{D}}^k} \left\{ \exp\left[-\frac{(y_{\text{D}}-y_{\text{D}0i})^2}{(t_{\text{D}}^n-\tau_{\text{D}})} \right] \Big/ \sqrt{(t_{\text{D}}^n-\tau_{\text{D}})} \right\} \cdot \int_{l_{\text{D}i}=0}^{l_{\text{D}i}=\Delta l_{\text{D}}} \left\{ \exp\left[-\frac{(x_{\text{D}}-x_{\text{D}0i})^2}{(t_{\text{D}}^n-\tau_{\text{D}})} \right] \Big/ \sqrt{(t_{\text{D}}^n-\tau_{\text{D}})} \right\} \cdot \left\{ 1 + 2\sum_{m=1}^{\infty} \exp\left[-\frac{m^2\pi^2(t_{\text{D}}^n-\tau_{\text{D}})}{z_{\text{eD}}^2} \right] \cos\frac{m\pi z_{\text{D}}}{z_{\text{eD}}} \cos\frac{m\pi z_{\text{D}0}(l_{\text{D}i})}{z_{\text{eD}}} \right\} \mathrm{d}l_{\text{D}i} \mathrm{d}\tau_{\text{D}} \tag{13}$$

Applying Eq. (13) to all the linear sources and arranging these equations into a matrix form give

$$\boldsymbol{p}_{\text{w}}^n - \boldsymbol{G}\boldsymbol{q}^n = \boldsymbol{D} \tag{14}$$

The matrices $\boldsymbol{G}$ and $\boldsymbol{D}$ are defined in Appendix B.

2.4. Wellbore storage and wellbore representation

In this work, the effect of wellbore storage on the pressure response is considered. Based on the method proposed by van Everdingen and Hurst (1949), the dimensionless wellbore storage equation is expressed as

$$1 - \frac{\gamma C_{\text{wD}}}{\Delta t_{\text{D}}^n} \left(p_{\text{wD}}^n - p_{\text{wD}}^{n-1} \right) = q_{\text{w-wbD}}^n \tag{15}$$

The bottomhole pressure is defined at the left surface of the 1st discretized linear source (see Fig. 2). According to Darcy's law (Darcy, 1856), the relationship between the dimensionless bottomhole pressure and the dimensionless pressure of the 1st discretized element can be expressed as

$$p_{\text{wbD}} - p_{\text{wD}} = \frac{2\beta h_{\text{D}} \Delta l_{\text{D}}}{k_{\text{D}} r_{\text{wD}}^2} q_{\text{w-wbD}}^n \tag{16}$$

2.5. Solution methodology

Based on pressure and flow continuity, the finite difference equations of the directional well (Eq. (10)), the analytical solution of the matrix system (Eq. (14)), the wellbore storage equation (Eq. (15)), and the wellbore representation equation (Eq. (16)) can be put together to form a system of linear equations. The system of linear equations can be written as

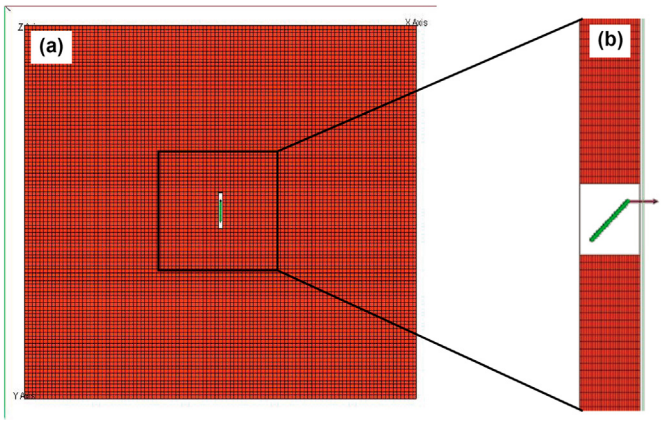

Fig. 3. Schematic of reservoir model built in the Eclipse. **(a)** Top view of the overall grid system; **(b)** Side view of the local grid system.

$$\begin{cases} \boldsymbol{A}\cdot\boldsymbol{p}_{\mathrm{w}}^{n}+\boldsymbol{B}_1\cdot\boldsymbol{q}^{n}-\boldsymbol{B}_2\cdot q_{\mathrm{w-wD}}^{n}=\boldsymbol{C}\cdot\boldsymbol{p}_{\mathrm{w}}^{n-1} \\ \boldsymbol{p}_{\mathrm{w}}^{n}-\boldsymbol{G}\boldsymbol{q}^{n}=\boldsymbol{D} \\ 1-\dfrac{\gamma C_{\mathrm{wD}}}{\Delta t_{\mathrm{D}}^{n}}\left(p_{\mathrm{wD}}^{n}-p_{\mathrm{wD}}^{n-1}\right)=q_{\mathrm{w-wD}}^{n} \\ p_{\mathrm{wD}}-p_{\mathrm{wbD}}=\dfrac{2\beta h_{\mathrm{D}}\Delta l_{\mathrm{D}}}{k_{\mathrm{D}}r_{\mathrm{wD}}^{2}}q_{\mathrm{w-wbD}}^{n} \end{cases} \tag{17}$$

In this system of linear equations, there are $2N_{\mathrm{w}}+2$ unknowns (N_{w} dimensionless pressure, N_{w} dimensionless withdrawal rates, 1 dimensionless bottomhole pressure, 1 dimensionless flux from well-element to wellbore) and $2N_{\mathrm{w}}+2$ linear equations (N_{w} well-flow equations, N_{w} matrix-flow equations, 1 wellbore-storge-effect equation, 1 flow equation from well-element to wellbore) at each timestep. Thus, the system of linear equations is closed and can be readily solved by using the Gaussian elimination method.

3. Validation against numerical software and analytical model

In this section, we demonstrate the validity of the proposed semi-analysis method by comparing its outputs against the results from commercial software (Eclipse). According to Holmes et al. (1998), the numerical software (Eclipse) can consider the non-uniform flux distribution by dividing the wellbore into several one-dimensional segments. In the Eclipse, the authors discrete the reservoir into $101 \times 101 \times 27$ grids, and the dimensions of each grid are $10 \times 17 \times 1$ m^3. Therefore, the reservoir is sufficiently large to avoid the boundary effect during production. Fig. 3 shows a top and a side view of the grid system, where a directional well locates at the center of the reservoir. The fluid and rock properties used in both the Eclipse model and the semi-analytical approach are consistently set as follows: $h = 27$ m, $\phi_{\mathrm{m}} = 0.2$, $c_{\mathrm{tm}} = 0.0012$ MPa^{-1}, $k_{\mathrm{m}} = 0.01$ mD, $k_{\mathrm{w}} = 3.16 \times 10^{11}$ mD, $c_{\mathrm{tw}} = 0$ MPa^{-1}, $C_{\mathrm{w}} = 0$ bbl/psi, $p_{\mathrm{i}} = 30$ MPa, $q_{\mathrm{w}} = 0.1$ m^3/d, $\mu = 1$ mPa s, $B = 0.985$ (dead oil), $r_{\mathrm{w}} = 0.05$ m, $L = 100$ m, and $\theta = 10°$. Moreover, for a more comprehensive comparison, the calculation results based on the assumption of Sousa and Moreno (2015) (i.e., the uniform flux distribution along the wellbore) are also presented in the validation. In their studies, the analytical solution of the slanted linear source well can be obtained by integrating the point source along the wellbore trajectory. Fig. 4 shows the pressure drops and pressure derivatives calculated by the proposed model, the model of Sousa and Moreno (2015), and numerical software. It can be seen that the calculation results from the proposed model are in excellent agreement with those of the numerical software, which demonstrates the validity of the proposed model. The pressure drops from the model of Sousa and Moreno (2015) are significantly larger than the other two, which shows the assumption of uniform flux can result in a significant error for field applications. Therefore, the proposed model with the non-uniform flux distribution can more accurately simulate the pressure transient behavior of the directional wells.

4. Results and discussion

In this section, the flux variations along the directional well under different inclined angles and wellbore radii are investigated. Subsequently, we distinguish all the flow regimes that can be observed during the production of a directional well. Finally, a comprehensive study was conducted to examine the pressure transient behavior of a directional well with different scenarios. The values of the dimensionless parameters of the benchmark model are as follows: $h_{\mathrm{D}} = 0.3$, $r_{\mathrm{wD}} = 1 \times 10^{-4}$, $C_{\mathrm{wD}} = 100$, $z_{\mathrm{D}} = 0.5$, $\theta = 6°$, $B = 0.985$, $\gamma = 4.27 \times 10^{-10}$, and $C_{\mathrm{s}} = 0$.

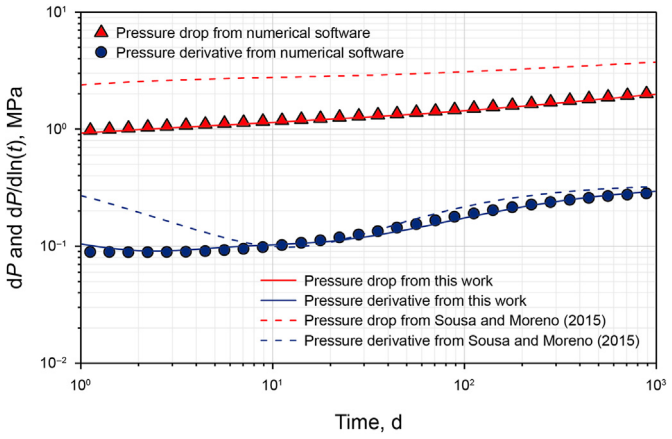

Fig. 4. Comparison of the pressure drops and pressure derivatives calculated by the proposed model, the model of Sousa and Moreno (2015), and the numerical software.

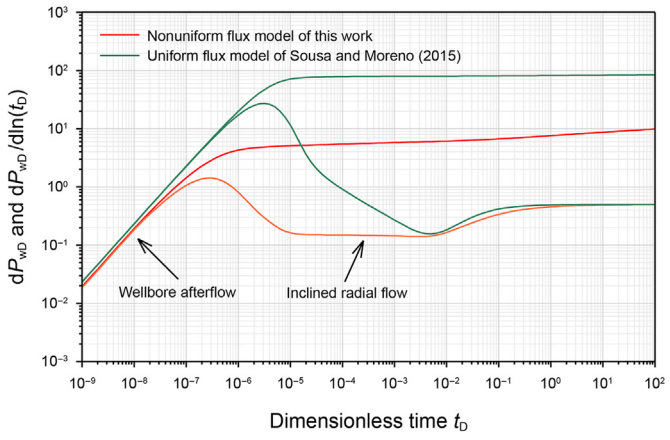

Fig. 5. Comparison between the pressure responses of the proposed model and the uniform flux model of Sousa and Moreno (2015).

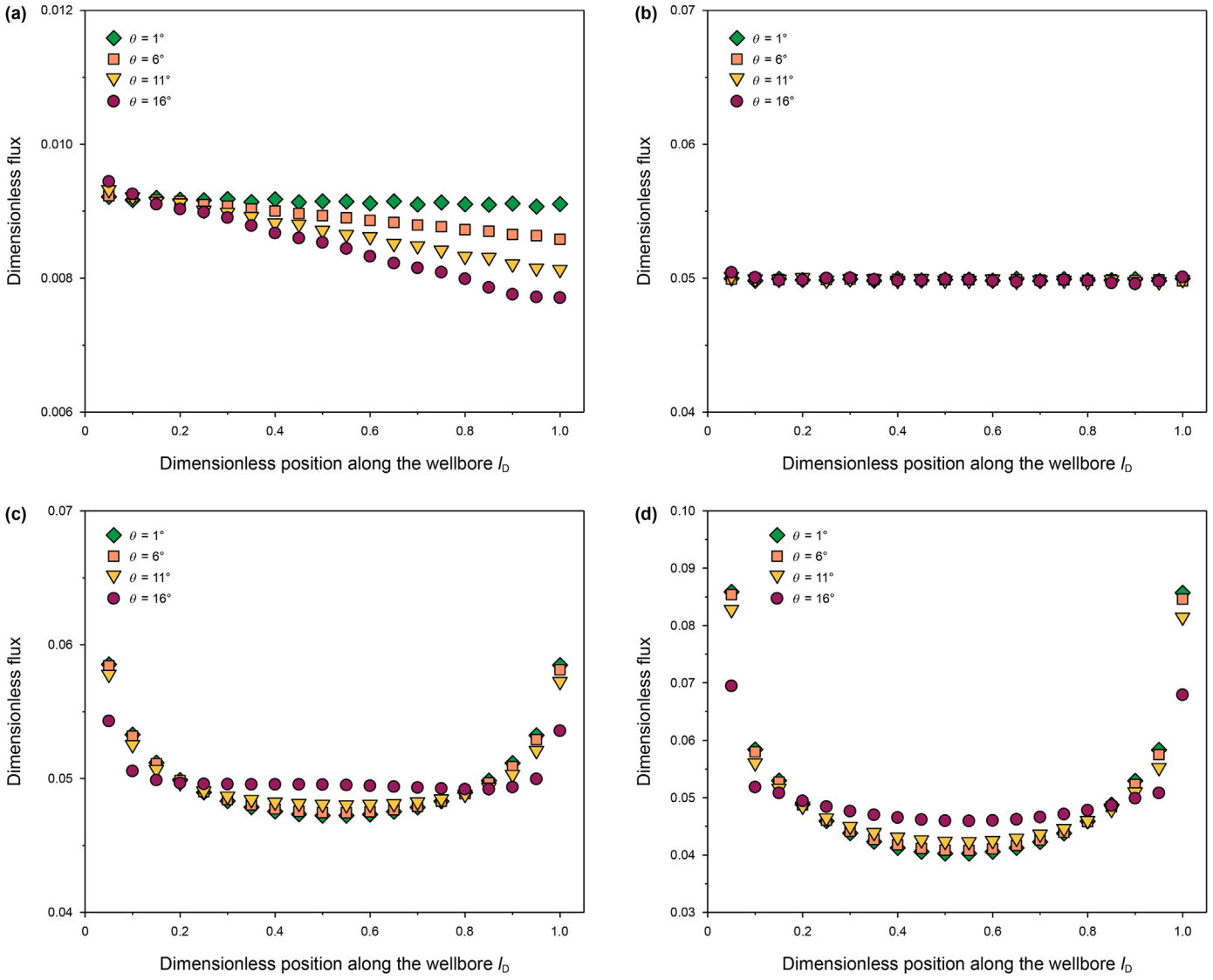

Fig. 6. Dimensionless flux distribution of the directional well with different inclined angles at different dimensionless times: (**a**) $t_D = 1 \times 10^{-8}$; (**b**) $t_D = 1 \times 10^{-4}$; (**c**) $t_D = 1 \times 10^{-1}$; (**d**) $t_D = 1 \times 10^{1}$.

4.1. Flux distribution along the directional well

In the existing studies, the uniform-flux models have been widely used for characterizing the transient flow behavior of the directional well. In these uniform-flux models, the directional well is represented with a single linear source and it was assumed that the flux variation along the directional well is neglected. In practice, the three-dimensional flow behavior in the vicinity of the wellbore should be physically present in the production period (Zhang and Yang, 2014; Teng and Li, 2019). Therefore, it is necessary to study the effect of the flux variation on the pressure responses in the entire production. Fig. 5 shows the comparison between the pressure responses of the proposed model and the uniform flux model of Sousa and Moreno (2015). As one can see in Fig. 5, both the pressure drop plots and the pressure derivative plots exhibit remarkable differences, implying that the flux variation along the direction well can significantly influence the simulation outputs. Besides, the inclined radial flow cannot be observed on the pressure derivative plots based on the assumption of uniform flux distribution. Since the flux variation can really be observed along the directional well, the assumption of uniform flux is an oversimplification for real cases, which can cause misidentification of flow regimes.

Moreover, we examine the effect of the inclined angle of the directional well on the flux distribution. Four inclined angles are considered, including $\theta = 1°$, 6°, 11°, and 16°. Fig. 6 shows the flux distribution along the directional well with different inclined angles and different dimensionless times (i.e., $t_D = 1 \times 10^{-8}$, 1×10^{-4}, 1×10^{-1}, and 1×10^{1}). As one can see in Fig. 6(a), at the early production period (wellbore afterflow), the dimensionless flux near the well heel is larger than that near the well toe. As the inclined angle is increased, the difference becomes more significant. This is ascribed to the effect of gravity, which can result in a lower pressure but higher flux near the well heel. The flux distribution in Fig. 6(b)

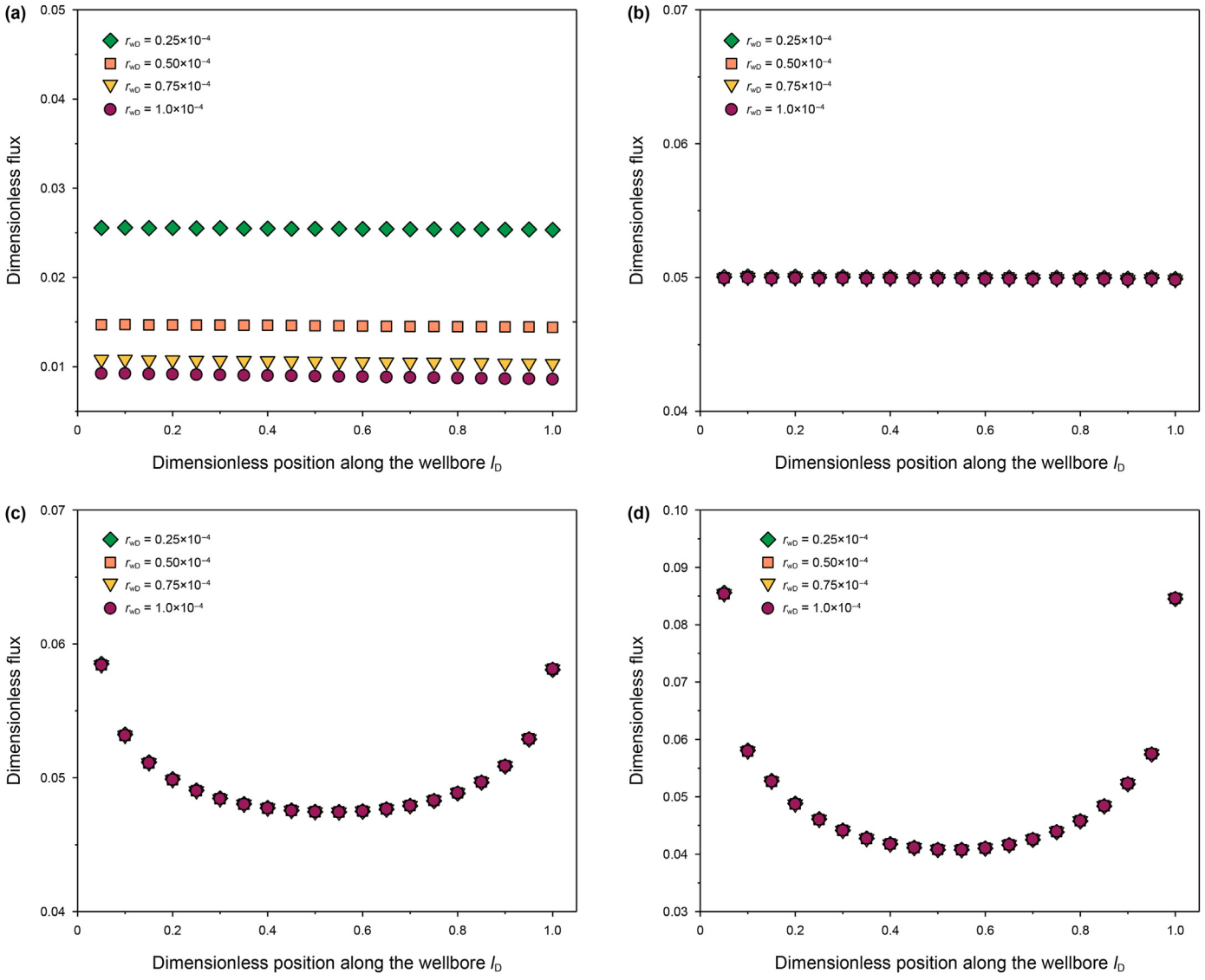

Fig. 7. Dimensionless flux distribution of the directional well with different wellbore radii at different dimensionless times: (**a**) $t_D = 1 \times 10^{-8}$; (**b**) $t_D = 1 \times 10^{-4}$; (**c**) $t_D = 1 \times 10^{-1}$; (**d**) $t_D = 1 \times 10^{1}$.

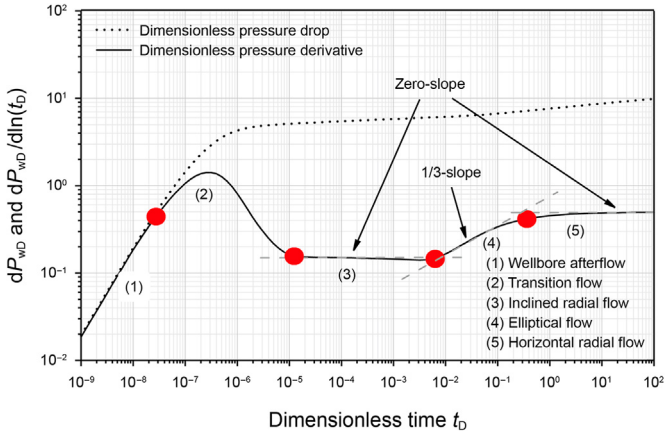

Fig. 8. Identification of the flow regimes that can be observed during the production of the benchmark model.

exhibits a slight difference, representing the appearance of radial flow around the directional well. Fig. 6(c) and (d) show the flux distribution during the late production period. A higher dimensionless flux can be observed near the well toe and heel, and a lower flux occurs at the middle part of the well.

Fig. 7 shows the dimensionless flux distribution of the directional well by varying the dimensionless wellbore radius from 0.25×10^{-4} to 1×10^{-4}. It is interesting to note that the influence of wellbore radius on the flux distribution can only be observed in the early production period with $t_D = 1 \times 10^{-8}$. In Fig. 7(a), a larger wellbore radius can induce a lower dimensionless flux distribution. This is because the wellbore storage effect is more significant with a larger wellbore radius, and the wellbore storage effect will prevent the fluid from entering the wellbore. The non-uniform flux distributions shown in Figs. 6 and 7 provide a further justification that the flux variations along the well trajectory should not be neglected to accurately model the transient flow behavior of a directional well.

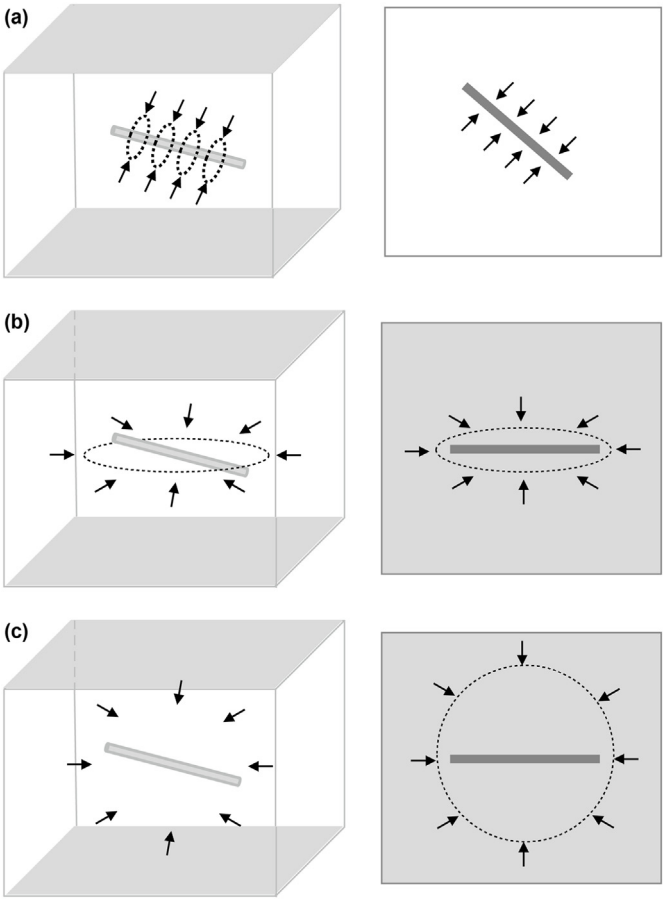

Fig. 9. The flow behavior of various flow regimes occurring during the production of the benchmark model: (**a**) Inclined radial flow from 3D view and side view; (**b**) Elliptical flow from 3D view and top view; (**c**) Horizontal radial flow from 3D view and top view.

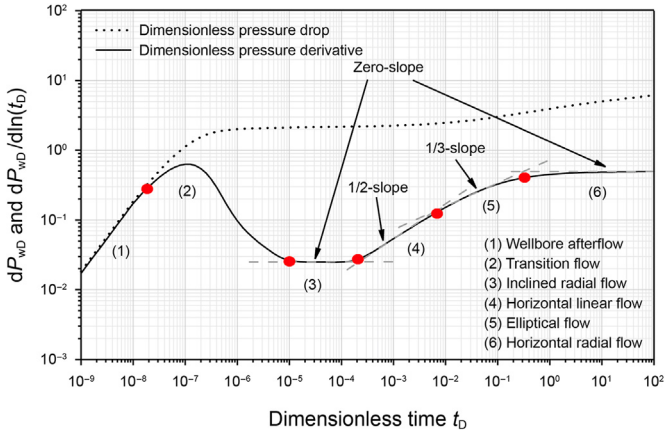

Fig. 10. Identification of the flow regimes that can be observed during the production of a horizontal well.

4.2. Flow regimes of a directional well

The flow regimes can be identified according to the slope on the pressure derivative curve. Fig. 8 presents the dimensionless pressure drop and pressure derivative of the benchmark directional well model that is calculated with the proposed semi-analytical approach. In this figure, five flow regimes can be distinguished, including (1) wellbore afterflow (1-slope), (2) transition flow (hump), (3) inclined radial flow (0-slope), (4) elliptical flow (1/3-slope), and (5) horizontal radial flow (0-slope). The wellbore afterflow occurs in the early production period, which reflects the effect of fluid elastic energy in the wellbore on the bottomhole pressure (Khatteb et al., 1991). The first 0-slope period on the diagram represents inclined radial flow, whose schematic is shown in Fig. 9(a) (Ozkan et al., 1999). During this period, the fluid near the wellbore flows radially to the directional well along the inclined direction. As the drainage area expands, the produced fluid can be from a further position than the near-well region, leading to an elliptical flow (see Fig. 9(b)). The elliptical flow presents a 1/3 slop on the pressure derivative curve (Teng and Li, 2018). Fig. 9(c) shows the schematic of horizontal radial flow, which can be observed during the late production period. On the pressure derivative curve, the second 0-slope region represents the horizontal radial flow (Sousa and Moreno, 2015).

Fig. 10 depicts the pressure drop and pressure derivative curves that are calculated with the proposed model with another set of parameters. The values of the parameters that are different from the benchmark model are as follows: $h_D = 0.05$ and $\theta = 0°$. It is noted that $\theta = 0°$ indicates that the well is horizontal, which can be regarded as a special directional well. Comparing Fig. 10 with Fig. 8, we can find that the main difference is that there is a 1/2-slope region appearing between the inclined radial flow and the elliptical flow on the pressure derivative curve. The 1/2-slope represents the occurrence of horizontal linear flow, which is schematically illustrated in Fig. 11 (Gill et al., 2007). In addition, the results in Figs. 8 and 10 imply that the horizontal linear flow can be observed only if the formation thickness is sufficiently small compared to the well length.

4.3. Sensitivity analysis

With the aid of the proposed model, a thorough sensitivity analysis is conducted to investigate the influences of wellbore storage, wellbore radius, inclined angle, well vertical position, and formation thickness on the pressure transient behavior of a directional well.

4.3.1. Wellbore storage

In this section, different dimensionless wellbore storage coefficients are investigated to explore their effects on the pressure-transient behavior of the directional well. Fig. 12 shows the pressure drop and pressure derivative curves obtained by varying C_{wD} from 1×10^2 to 1×10^5 with the proposed model. As shown in this figure, the wellbore storage mainly affects the early stage of production. The wellbore afterflow regime is diagnosed as a straight line with one slope on the pressure derivative curve, and different wellbore storage coefficients are shown as a group of curve clusters parallel to each other in Fig. 12. With the increase of the wellbore storage coefficient, the duration of the wellbore afterflow regime becomes longer and the pressure drop becomes smaller. Furthermore, the wellbore storage can exert a significant effect on the inclined radial flow. For example, for the scenario of $C_{wD} = 1 \times 10^5$, the inclined radial flow cannot be identified on the pressure derivative curve because it is covered by the wellbore afterflow. In addition, if the dimensionless time is sufficiently large (e.g., $t_D > 1 \times 10^{-2}$), the pressure derivative curves of different dimensionless wellbore storage coefficients exhibit negligible differences.

4.3.2. Wellbore radius

To examine the effect of wellbore radius on the pressure transient behavior of a directional well, different dimensionless wellbore radii are considered, including $r_{wD} = 0.5 \times 10^{-4}$, 1×10^{-4},

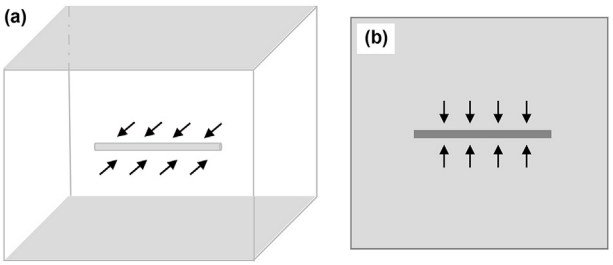

Fig. 11. The flow behavior of an exclusive flow regime occurring during the production of a horizontal well: horizontal linear flow from 3D view (**a**) and top view (**b**).

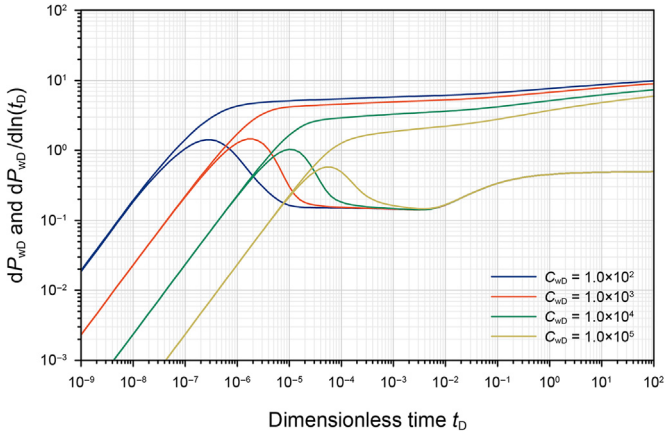

Fig. 12. Impact of wellbore storage on the pressure drops and pressure derivatives of a directional well.

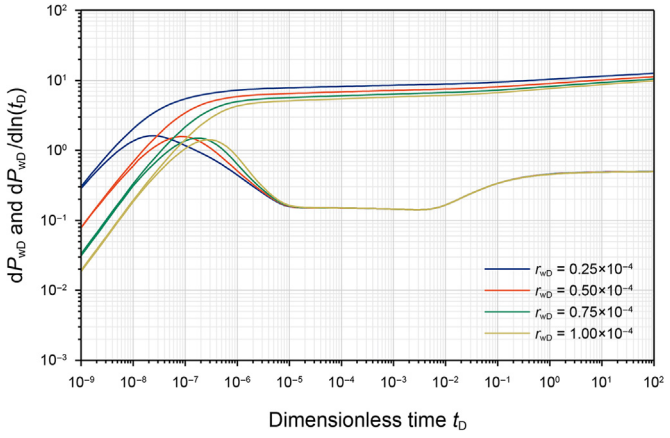

Fig. 13. Impact of wellbore radius on the pressure drops and pressure derivatives of a directional well.

1.5×10^{-4}, and 2×10^{-4}. The pressure drops and pressure derivatives calculated by the proposed model with different wellbore radii are shown in Fig. 13. As one can see in Fig. 13, the wellbore radius mainly influences the early production period, and its influence on the pressure transient behavior is similar to the wellbore storage. This is because wellbore storage represents the magnitude of fluid elastic energy within the wellbore. A larger wellbore radius leads to a larger volume of fluid in the wellbore, as well as a larger wellbore storage effect. Therefore, as the dimensionless wellbore

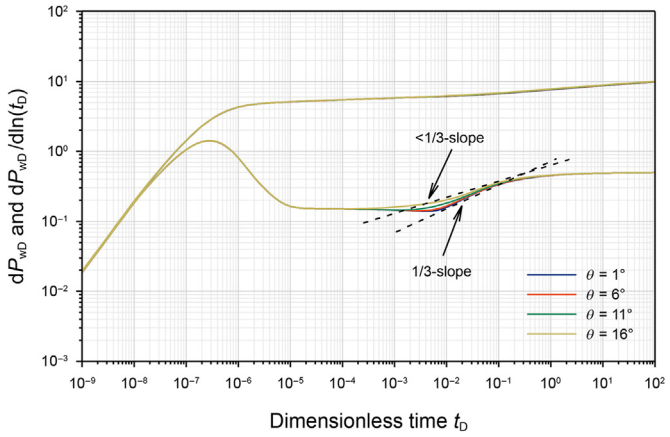

Fig. 14. Impact of smaller inclined angle change on the pressure drops and pressure derivatives of a directional well.

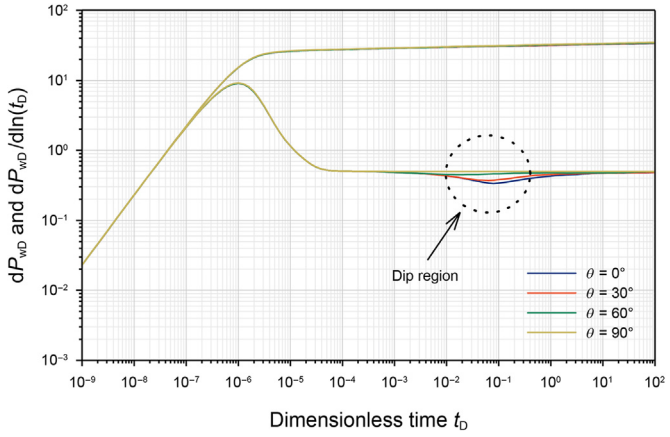

Fig. 15. Impact of larger inclined angle change on the pressure drops and pressure derivatives of a directional well.

radius is increased, the during of the wellbore afterflow is increased.

4.3.3. Inclined angle

Fig. 14 demonstrates the pressure response of a directional well with different inclined angles (i.e., $\theta = 1°$, 6°, 11°, and 16°). It can be found in Fig. 14 that the inclined angle mainly influences the elliptical flow period. As the inclined angle is increased, the slope on the pressure derivative curve is decreased, and the elliptical flow is less pronounced. This is due to the interference from the lower and upper boundaries. If the inclined angle is sufficiently large, the interference from the lower and upper boundaries can change the fluid streamlines before the occurrence of the elliptical flow. In addition to the benchmark reservoir model, a reservoir model with a larger formation thickness ($h_D = 1$) is considered to explore the effect of the inclined angle on the pressure transient behavior of a direction well. Fig. 15 presents the pressure changes and pressure derivatives of a direction well model by varying the inclined angle from 0° to 90° with $h_D = 1$. It is noted that, for the scenario of $h_D = 1$, although the inclined angle of the directional well is varied from 0° to 90°, the well will not penetrate beyond the upper and lower boundaries. Comparing Fig. 15 with Fig. 14, one can find that the transition between the inclined radial flow and the horizontal

radial flow is changed from a positive-slope region to a dip region as the formation thickness is increased. The dip region in Fig. 15 indicates a three-dimensional (3D) flow near the wellbore. For example, the 3D spherical flow will induce a −1/2 slope on the pressure derivative curve. Since a larger inclined angle is more favorable for causing a 2D-type flow (e.g., for the case of $\theta = 90°$, the well is vertical and flow can be simplified to 2D), the dip region in Fig. 15 is more noticeable for a smaller inclined angle.

4.3.4. Vertical position

In real field cases, the directional well may not be located at the center along the vertical direction. Thus, in this section, we explore the effect of the vertical position on the pressure transient behavior of a direction well. The vertical position in this section is characterized by a dimensionless parameter z_{wD}, which is defined as

$$z_{wD} = \frac{z_w}{h} \tag{18}$$

In Eq. (18), z_w indicates the distance between the center of the directional well and the upper reservoir boundary. According to the definition of z_{wD}, $z_{wD} = 0.5$ represents that direction well is located at the center along the vertical direction, and a smaller value of z_{wD} indicates that the well is nearer to the upper boundary. The pressure response curves of the directional well with different z_{wD} (i.e., $z_{wD} = 0.2$, 0.3, 0.4, and 0.5) are shown in Fig. 16. In Fig. 16, the effect of the well vertical position can be observed between the inclined radial flow period and the elliptical flow period. If the directional well is nearer to the upper boundary, the inclined radial flow will terminate earlier due to the boundary effect. Therefore, one can observe a longer transition period between the inclined radial flow and the elliptical flow with a smaller value of z_{wD}.

4.3.5. Formation thickness

Fig. 17 depicts the effect of formation thickness on the pressure transient behavior of a directional well. In Fig. 17, the dimensionless formation thickness is varied from 0.2 to 0.5. It is worth noting that, a larger dimensionless formation thickness leads to a larger value of dimensionless pressure drop. This is because the dimensionless pressure drop is proportional to the formation thickness according to Eq. (1). But this does not imply that the physical wellbore pressure will undergo a higher drop in a thicker formation. In addition, on the pressure derivative curves, the inclined radial flow perpendicular to the wellbore is maintained for a longer time with a larger formation thickness. This is due to the fact that the distance between the well and the top-bottom boundary becomes longer and the time for the pressure front to reach the boundary will be increased.

4.4. Application of the proposed model to a field example

In this section, the proposed model is used to fit the pressure buildup data from a directional well, which is deviated 52° from the horizontal direction. The well was produced at 3.28 m^3/d for three days, followed by a four-day pressure buildup. The other known data of the reservoir and well are given in Table 1. The unknown parameters (including the matrix permeability and the wellbore storage coefficient) can be determined by the history matching of the test data. Fig. 18 presents a log-log plot of the measured pressure data and simulated ones. It can be seen that the calculated pressure buildup data is in excellent well with the measured pressure buildup data, such that the values of unknown parameters

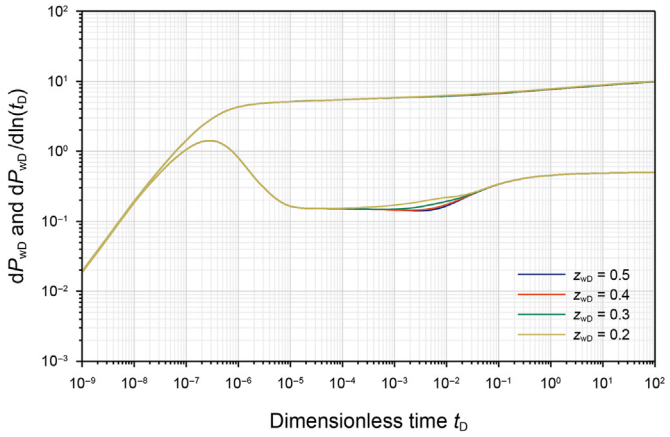

Fig. 16. Impact of vertical position on the pressure drops and pressure derivatives of a directional well.

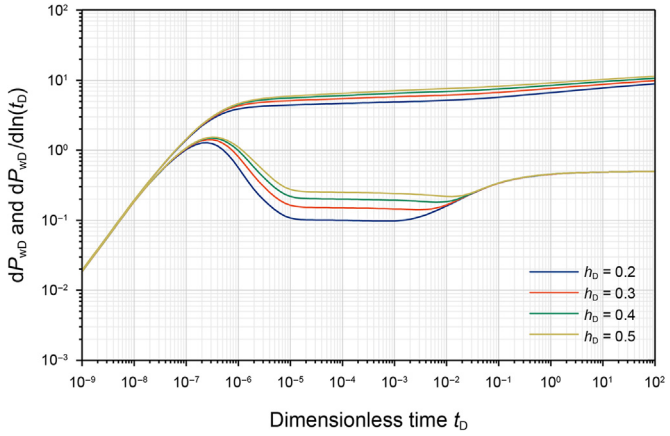

Fig. 17. Impact of formation thickness on the pressure drops and pressure derivatives of a directional well.

can be also obtained (see Table 2). Besides, the wellbore afterflow and radial flow can be significantly identified in Fig. 18.

5. Conclusions

This paper applies a novel semi-analytical model to research the pressure transient behavior of directional wells. With the aid of the proposed model, we consider the effect of flux variation on pressure dynamics and distinguish the flow regimes appearing in directional wells during production. Moreover, the effects of wellbore storage, wellbore radius, inclined angle, vertical position, and formation thickness on pressure response are studied. The calculation results lead us to draw the following conclusions:

- The flux distribution along the directional well is non-uniform. During the late production, subject to the horizontal radial flow, the flux distribution is higher at the well toe and heel and lower in the well middle.
- For a given reservoir condition, a directional well may exhibit the following flow regimes: wellbore afterflow, transition flow, inclined radial flow, horizontal linear flow, elliptical flow, and horizontal radial flow. Horizontal linear flow can be

Table 1
Known data of the reservoir and well in a real field example.

Parameter	Value	Parameter	Value
q_w, m^3/d	3.28	c_{tm}, MPa^{-1}	1.216×10^{-3}
h, m	5.5	ϕ_m	0.15
B, m^3/m^3	1.0974	r_w, m	0.07
μ, mPa s	4.6	θ, °	52

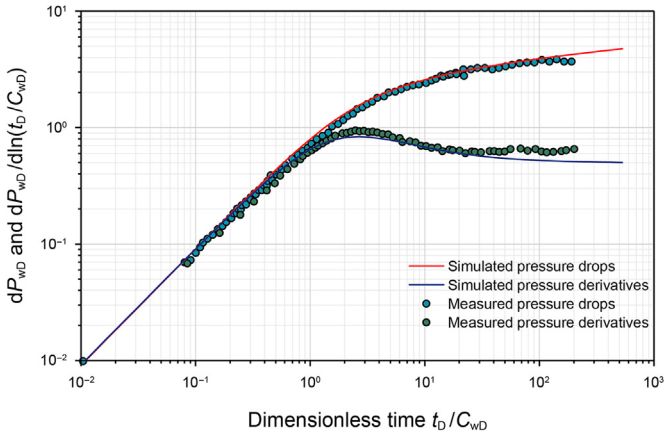

Fig. 18. Comparison of the measured pressure data and calculated ones using the history-matched model.

Table 2
History matching results for the pressure buildup data.

Parameter	Value	Parameter	Value
k_m, mD	1.3	C_w, m^3 MPa^{-1}	0.016

observed on the pressure derivative curve of a horizontal well only if the formation thickness is sufficiently small compared to the well length.

- A larger wellbore storage coefficient, as well as a larger wellbore radius, tends to result in a smaller pressure drop and a longer duration of the wellbore afterflow regime.
- For the case of a smaller formation thickness ($h_D = 0.3$), as the increasing inclined angle, the slope of the elliptical flow on the pressure derivative curve decreases. For the case of a larger formation thickness ($h_D = 1$), a smaller inclined angle will induce the 3D spherical flow, whereas a larger inclined angle is more conducive to causing a 2D radial flow.
- The inclined radial flow is maintained for a longer time with the increase in formation thickness and the value of z_{wD}.

The practical importance of this work is the advancement of the pressure transient analysis of the directional well subject to flux variation. With the aid of the semi-analytical method, this work has high computational efficiency on the basis of ensuring the accuracy of the model. In addition, the proposed model is suitable for fully penetrating and partially penetrating directional wells. Future work will improve the method for application to complex formation conditions, including anisotropic and heterogeneous reservoirs and various outer boundaries.

CRediT authorship contribution statement

Yan-Zhong Liang: Formal analysis, Validation, Writing – original draft. **Bai-Lu Teng:** Conceptualization, Supervision. **Wan-Jing Luo:** Conceptualization, Writing – review & editing.

Declaration of competing interest

The authors declare that they have no known competing financial interests or personal relationships that could have appeared to influence the work reported in this paper.

Acknowledgments

The authors would like to acknowledge the financial support provided by the National Natural Science Foundation of China (No. 52104043).

Appendix A. Numerical formulation for the oil flow in the wellbore system

In this work, the governing equation describing the seepage phenomenon occurring in the wellbore system is written as

$$\frac{\partial^2 p_w}{\partial l^2} + \frac{B\mu q}{\beta \Delta l A k_w} = \frac{\mu \phi_w c_{tw}}{\beta k_w} \frac{\partial p_w}{\partial t} \tag{A-1}$$

The dimensionless form of Eq. (A-1) is expressed as

$$\frac{\partial^2 p_{wD}}{\partial l_D^2} - \frac{2h_D}{k_D \Delta l_D r_{wD}^2} q_D^n = \frac{C_s}{k_D} \frac{\partial p_{wD}}{\partial t_D} \tag{A-2}$$

Applying the finite-difference approximation to the first term on the left-hand side of Eq. (A-2) at the time level t_D^n, then we can have

$$\begin{aligned} \frac{\partial^2 p_{wD}}{\partial l_D^2} &\approx \frac{1}{\Delta l_D} \left[\left(\frac{\partial p_{wD}^n}{\partial l_D} \right)_{i+1/2} - \left(\frac{\partial p_{wD}^n}{\partial l_D} \right)_{i-1/2} \right] \\ &\approx \frac{1}{\Delta l_D} \left(\frac{p_{wD_{i+1}}^n - p_{wD_i}^n}{\Delta l_{D_{i+1/2}}} - \frac{p_{wD_i}^n - p_{wD_{i-1}}^n}{\Delta l_{D_{i-1/2}}} \right) \end{aligned} \tag{A-3}$$

Considering the discrete well elements have a uniform dimension in this work, Eq. (A-3) can be written as

$$\frac{\partial^2 p_{wD}}{\partial l_D^2} = \frac{1}{\Delta l_D^2} \left(p_{wD_{i+1}}^n - 2p_{wD_i}^n + p_{wD_{i-1}}^n \right) \tag{A-4}$$

Similarly, the first term on the right-hand side of Eq. (A-2) can be written as

$$\frac{C_s}{k_D} \frac{\partial p_{wD}}{\partial t_D} = \frac{C_s}{k_D} \frac{1}{\Delta t_D^n} \left(p_{wD_i}^n - p_{wD_i}^{n-1} \right) \tag{A-5}$$

Substituting Eqs. (A-3) and (A-5) into Eq. (A-2), we can have

$$\frac{1}{\Delta l_D^2}\left(p^n_{wD_{i+1}} - 2p^n_{wD_i} + p^n_{wD_{i-1}}\right) + \frac{2h_D}{k_D \Delta l_D r^2_{wD}} q^n_{D_i} = \frac{C_s}{k_D}\frac{1}{\Delta t^n_D}\left(p^n_{wD_i} - p^{n-1}_{wD_i}\right) \tag{A-6}$$

Merging similar terms of Eq. (A-6), we can have

$$\left(\frac{2}{\Delta l_D^2} + \frac{C_s}{k_D}\frac{1}{\Delta t^n_D}\right)p^n_{wD_i} - \frac{1}{\Delta l_D^2}p^n_{wD_{i+1}} - \frac{1}{\Delta l_D^2}p^n_{wD_{i-1}} + \frac{2h_D}{k_D \Delta l_D r^2_{wD}} q^n_{D_i} = \frac{C_s}{k_D}\frac{1}{\Delta t^n_D}p^{n-1}_{wD_i} \tag{A-7}$$

For convenience, we define the following parameters:

$$a_{i+1} = a_{i-1} = \frac{1}{\Delta l_D^2},\quad b = \frac{2h_D}{k_D \Delta l_D r^2_{wD}},\quad c = \frac{C_s}{k_D}\frac{1}{\Delta t^n_D} \tag{A-8}$$

$$A_i = a_{i+1} + a_{i-1} + c \tag{A-9}$$

$$\text{A point source function in } 3-\text{D} = \text{A linear source function in the } x \text{ direction} \times \text{A linear source function in the } y \text{ direction} \times \text{A linear source function in the } z \text{ direction} \tag{B-1}$$

It's worth noting that

$$\begin{cases} i = 1, & a_{i-1} = 0 \\ i = N_w, & a_{i+1} = 0 \end{cases} \tag{A-10}$$

As such, the approximated flow equation for the well element controlling output should be written as

$$A_i p^n_{wD_i} - a_{i+1}p^n_{wD_{i+1}} - a_{i-1}p^n_{wD_{i-1}} + b\left(q^n_{D_i} - q^n_{w-wD_i}\right) = cp^{n-1}_{wD_i} \tag{A-11}$$

Applying Eq. (A-11), the flow equations for the N_w well elements can be written in a matrix format:

$$\boldsymbol{A} \odot \boldsymbol{p}^n_w + \boldsymbol{B}_1 \odot \boldsymbol{q}^n - \boldsymbol{B}_2 \odot q^n_{w-wD} = \boldsymbol{C} \odot \boldsymbol{p}^{n-1}_w \tag{A-12}$$

where $\odot$ is the Hadamard product operator, and $\boldsymbol{A}$ is the matrix of the coefficients $\boldsymbol{A}_i$. The matrix $\boldsymbol{p}^n_w$, $\boldsymbol{B}_1$, $\boldsymbol{q}^n$, and $\boldsymbol{B}_2$ are detailed as follows:

$$\boldsymbol{p}^n_w = \begin{bmatrix} p^n_{w_1} \\ \vdots \\ p^n_{w_{iw}} \\ \vdots \\ p^n_{w_{Nw}} \end{bmatrix},\ \boldsymbol{B}_1 = \begin{bmatrix} b \\ \vdots \\ b \end{bmatrix},\ \boldsymbol{q}^n = \begin{bmatrix} q^n_{w_1} \\ \vdots \\ q^n_{w_{iw}} \\ \vdots \\ q^n_{w_{Nw}} \end{bmatrix},\ \boldsymbol{B}_2 = \begin{bmatrix} 0 \\ \vdots \\ b \\ \vdots \\ 0 \end{bmatrix},\ \boldsymbol{C} = \begin{bmatrix} c \\ \vdots \\ c \end{bmatrix} \tag{A-13}$$

where the iw indicates the location of the wellbore element. The position of constant b in matrix $\boldsymbol{B}_2$ is consistent with the position of pressure $p^n_{w_{iw}}$ in matrix $\boldsymbol{p}^n_f$.

Appendix B. Analytical solution for the oil flow in the matrix system

Introduced by Carslaw and Jaeger (1959) and Gringarten and Ramey (1973), an instantaneous point source pressure function in a three-dimensional reservoir can be described by the Newman product method as

where the instantaneous linear source function in the x and y directions have the same form, and the function in the x-direction at time t is given as follows:

$$\frac{\phi c[p_i - p(x(y),t)]}{\delta} = \exp\left[-\frac{(x-x_0)^2}{4\alpha t}\right] \Big/ \sqrt{4\pi\alpha t} \tag{B-2}$$

where δ is the instantaneous flux, α is diffusivity which is defined as $\alpha = k_m/\mu\phi_m c_t$. Similarly, the instantaneous linear source function used to describe bounded reservoir in the z-direction at time t is

$$\frac{\phi c[p_i - p(z,t)]}{\delta} = \frac{1}{z_e}\left\{1 + 2\sum_{m=1}^{\infty}\exp\left[-\frac{m^2\pi^2\alpha(t-\tau)}{z_e^2}\right]\cos\frac{m\pi z}{z_e}\cos\frac{m\pi z_0}{z_e}\right\} \tag{B-3}$$

where τ presents the time when the source function is activated. Inserting Eqs. (B-2) and (B-3) into Eq. (B-1) can obtain the instantaneous point source function in a three-dimensional single-layer reservoir:

$$p_i - p(x,y,z,t) = \frac{\delta}{\phi_m c_{tm}} \cdot \exp\left[-\frac{(x-x_0)^2}{4\alpha t}\right] \Big/ \sqrt{4\pi\alpha t} \cdot \exp\left[-\frac{(y-y_0)^2}{4\alpha t}\right] \Big/ \sqrt{4\pi\alpha t} \cdot \frac{1}{z_e}\left\{1 + 2\sum_{m=1}^{\infty}\exp\left[-\frac{m^2\pi^2\alpha(t-\tau)}{z_e^2}\right]\cos\frac{m\pi z}{z_e}\cos\frac{m\pi z_0}{z_e}\right\} \tag{B-4}$$

where x_0, y_0, and z_0 represent the position of the point source along with the x, y, and z directions, and z_e represents the reservoir size along with the z directions. By integrating Eq. (B-4), the linear source function along the inclined direction is obtained

$$p_i - p(x,y,z,t) = \frac{\delta}{\phi_m c_{tm}} \frac{1}{z_e} \cdot \left\{ \exp\left[-\frac{(y-y_{0i})^2}{4\alpha(t-\tau)} \right] \Big/ \sqrt{4\pi\alpha(t-\tau)} \right\} \cdot \int_{l_i=0}^{l_i=\Delta l} \left\{ \exp\left[-\frac{(x-x_0(l_i))^2}{4\alpha(t-\tau)} \right] \Big/ \sqrt{4\pi\alpha(t-\tau)} \right\} \cdot \left\{ 1 + 2\sum_{m=1}^{\infty} \exp\left[-\frac{m^2\pi^2\alpha(t-\tau)}{z_e^2} \right] \cos\frac{m\pi z}{z_e} \cos\frac{m\pi z_0(l_i)}{z_e} \right\} dl_i \tag{B-5}$$

where Δl is the wellbore-element length along the inclination direction; l_i represents the spatial position of the wellbore element (i); $x_0(l_i)$ and $z_0(l_i)$ represent the space coordinates of the wellbore element (i) in x and z directions. By integrating over time, the linear source function with a constant withdrawal rate of q is obtained

$$p_i - p(x,y,z,t) = \frac{Bq}{\phi_m c_{tm} \Delta l} \frac{1}{z_e} \int_{\tau_1}^{\tau_2} \left\{ \exp\left[-\frac{(y-y_0)^2}{4\alpha(t-\tau)} \right] \Big/ \sqrt{4\pi\alpha(t-\tau)} \right\} \cdot \int_{l_i=0}^{l_i=\Delta l} \left\{ \exp\left[-\frac{(x-x_0(l_i))^2}{4\alpha(t-\tau)} \right] \Big/ \sqrt{4\pi\alpha(t-\tau)} \right\} \cdot \left\{ 1 + 2\sum_{m=1}^{\infty} \exp\left[-\frac{m^2\pi^2\alpha(t-\tau)}{z_e^2} \right] \cos\frac{m\pi z}{z_e} \cos\frac{m\pi z_0(l_i)}{z_e} \right\} dl_i d\tau \tag{B-6}$$

where (τ_1, τ_2) represents the linear source lasting from the time τ_1 to time τ_2. Besides, the withdrawal rate of a wellbore element varies with time. With the aid of the superposition principle, we can calculate the pressure response caused by a linear source that has a flux rate varying with time:

$$p_i - p(x,y,z,t^n) = \frac{B}{\phi_m c_{tm} \Delta l} \frac{1}{z_e} \sum_{k=1}^{n} q^k \int_{t^{k-1}}^{t^k} \left\{ \exp\left[-\frac{(y-y_0)^2}{4\alpha(t^n-\tau)} \right] \Big/ \sqrt{4\pi\alpha(t^n-\tau)} \right\} \cdot \int_{l_i=0}^{l_i=\Delta l} \left\{ \exp\left[-\frac{(x-x_0(l_i))^2}{4\alpha(t^n-\tau)} \right] \Big/ \sqrt{4\pi\alpha(t^n-\tau)} \right\} \cdot \left\{ 1 + 2\sum_{m=1}^{\infty} \exp\left[-\frac{m^2\pi^2\alpha(t^n-\tau)}{z_e^2} \right] \cos\frac{m\pi z}{z_e} \cos\frac{m\pi z_0(l_i)}{z_e} \right\} dl_i d\tau \tag{B-7}$$

The pressure response caused by a single-linear source has been obtained. However, the directional well is discretized into N_w elements. Therefore, we should sum up the pressure response from all of the elements to obtain the pressure response caused by the entire directional well, and the equation is expressed as

$$p_{\mathrm{i}}-p(x,y,z,t^n)=\frac{B}{\phi_{\mathrm{m}}c_{\mathrm{tm}}\Delta l}\frac{1}{z_e}\sum_{i=1}^{N_{\mathrm{w}}}\sum_{k=1}^{n}q_i^k\int_{t^{k-1}}^{t^k}\left\{\exp\left[-\frac{(y-y_{0i})^2}{4\alpha(t^n-\tau)}\right]\Big/\sqrt{4\pi\alpha(t^n-\tau)}\right\}\cdot\int_{l_i=0}^{l_i=\Delta l}\left\{\exp\left[-\frac{(x-x_0(l_i))^2}{4\alpha(t^n-\tau)}\right]\Big/\sqrt{4\pi\alpha(t^n-\tau)}\right\}\cdot\left\{1+2\sum_{m=1}^{\infty}\exp\left[-\frac{m^2\pi^2\alpha(t^n-\tau)}{z_{\mathrm{e}}^2}\right]\cos\frac{m\pi z}{z_{\mathrm{e}}}\cos\frac{m\pi z_0(l_i)}{z_{\mathrm{e}}}\right\}\mathrm{d}l_i\mathrm{d}\tau \tag{B-8}$$

Rewriting Eq. (B-8) into a dimensionless form, we can obtain

$$p_{\mathrm{wD}}(x_{\mathrm{D}},y_{\mathrm{D}},z_{\mathrm{D}},t_{\mathrm{D}}^n)=\frac{h_{\mathrm{D}}}{2\Delta l_{\mathrm{D}}}\frac{1}{z_{\mathrm{eD}}}\sum_{i=1}^{N_{\mathrm{w}}}\sum_{k=1}^{n}q_{\mathrm{D}i}^k\int_{t_{\mathrm{D}}^{k-1}}^{t_{\mathrm{D}}^k}\left\{\exp\left[-\frac{(y_{\mathrm{D}}-y_{\mathrm{D}0i})^2}{(t_{\mathrm{D}}^n-\tau_{\mathrm{D}})}\right]\Big/\sqrt{(t_{\mathrm{D}}^n-\tau_{\mathrm{D}})}\right\}\cdot\int_{l_{\mathrm{D}i}=0}^{l_{\mathrm{D}i}=\Delta l_{\mathrm{D}}}\left\{\exp\left[-\frac{(x_{\mathrm{D}}-x_{\mathrm{D}0i})^2}{(t_{\mathrm{D}}^n-\tau_{\mathrm{D}})}\right]\Big/\sqrt{(t_{\mathrm{D}}^n-\tau_{\mathrm{D}})}\right\}\cdot\left\{1+2\sum_{m=1}^{\infty}\exp\left[-\frac{m^2\pi^2(t_{\mathrm{D}}^n-\tau_{\mathrm{D}})}{z_{\mathrm{eD}}^2}\right]\cos\frac{m\pi z_{\mathrm{D}}}{z_{\mathrm{eD}}}\cos\frac{m\pi z_{\mathrm{D}0}(l_{\mathrm{D}i})}{z_{\mathrm{eD}}}\right\}\mathrm{d}l_{\mathrm{D}i}\mathrm{d}\tau_{\mathrm{D}} \tag{B-9}$$

For simplifying Eq. (B-9), we define that

$$G_i^k\left(x,y,z,t_{\mathrm{D}}^k\right)=\frac{h_{\mathrm{D}}}{2\Delta l_{\mathrm{D}}}\frac{1}{z_{\mathrm{eD}}}\int_{t_{\mathrm{D}}^{k-1}}^{t_{\mathrm{D}}^k}\left\{\exp\left[-\frac{(y_{\mathrm{D}}-y_{\mathrm{D}0i})^2}{(t_{\mathrm{D}}^n-\tau_{\mathrm{D}})}\right]\Big/\sqrt{(t_{\mathrm{D}}^n-\tau_{\mathrm{D}})}\right\}\cdot\int_{l_{\mathrm{D}i}=0}^{l_{\mathrm{D}i}=\Delta l_{\mathrm{D}}}\left\{\exp\left[-\frac{(x_{\mathrm{D}}-x_{\mathrm{D}0i})^2}{(t_{\mathrm{D}}^n-\tau_{\mathrm{D}})}\right]\Big/\sqrt{(t_{\mathrm{D}}^n-\tau_{\mathrm{D}})}\right\}\cdot\left\{1+2\sum_{m=1}^{\infty}\exp\left[-\frac{m^2\pi^2(t_{\mathrm{D}}^n-\tau_{\mathrm{D}})}{z_{\mathrm{eD}}^2}\right]\cos\frac{m\pi z_{\mathrm{D}}}{z_{\mathrm{eD}}}\cos\frac{m\pi z_{\mathrm{D}0}(l_{\mathrm{D}i})}{z_{\mathrm{eD}}}\right\}\mathrm{d}l_{\mathrm{D}i}\mathrm{d}\tau_{\mathrm{D}} \tag{B-10}$$

As such, Eq. (B-9) is rewritten as

$$p_{\mathrm{wD}}(x_{\mathrm{D}},y_{\mathrm{D}},z_{\mathrm{D}},t_{\mathrm{D}}^n)=\sum_{i=1}^{N_{\mathrm{w}}}\sum_{k=1}^{n}q_{\mathrm{D}i}^kG_i^k\left(x,y,z,t_{\mathrm{D}}^k\right) \tag{B-11}$$

Note that at each time step, the term G_i^k can be easily calculated because all the parameters are known. Subsequently, we apply Eq. (B-11) to all of the wellbore elements and arrange these matrix flow equations into a matrix format. Eq. (B-11) can be rewritten as

$$\boldsymbol{p}_{\mathrm{w}}^n-\boldsymbol{G}\boldsymbol{q}^n=\boldsymbol{D} \tag{B-12}$$

where the matrices of $\boldsymbol{G}$ and $\boldsymbol{D}$ are as follows:

$$\boldsymbol{G}=\begin{bmatrix}G_1^k\left(1,t_{\mathrm{D}}^k\right)&\cdots&G_{N_{\mathrm{w}}}^k\left(1,t_{\mathrm{D}}^k\right)\\ \vdots&\ddots&\vdots\\ G_1^k\left(N_{\mathrm{w}},t_{\mathrm{D}}^k\right)&\cdots&G_{N_{\mathrm{w}}}^k\left(N_{\mathrm{w}},t_{\mathrm{D}}^k\right)\end{bmatrix},\ \boldsymbol{D}=\begin{bmatrix}\sum_{i=1}^{N_{\mathrm{w}}}\sum_{k=1}^{n}q_{\mathrm{D}i}^kG_i^k\left(I,t_{\mathrm{D}}^k\right)\\ \vdots\\ \sum_{i=1}^{N_{\mathrm{w}}}\sum_{k=1}^{n}q_{\mathrm{D}i}^kG_i^k\left(I,t_{\mathrm{D}}^k\right)\end{bmatrix} \tag{B-13}$$

References

Albattat, R., AlSinan, M., Kwak, H., Hoteit, H., 2022. Modeling lost-circulation in natural fractures using semi-analytical solutions and type-curves. J. Petrol. Sci. Eng. 216, 110770. https://doi.org/10.1016/j.petrol.2022.110770.

Al-Kabbawi, F.A., 2022. The optimal semi-analytical modeling for the infinite-conductivity horizontal well performance under rectangular bounded reservoir based on a new instantaneous source function. Petroleum. https://doi.org/10.1016/j.petlm.2022.04.005.

Bond, A., Zhu, D., Kamkom, R., 2006. The effect of well trajectory on horizontal well performance. In: SPE International Oil and Gas Conference and Exhibition in China. https://doi.org/10.2118/104183-MS.

Carslaw, H.S., Jaeger, J.C., 1959. In: Conduction of Heat in Solids, second ed. Oxford University Press, Oxford, UK.

Cinco, H., Miller, F.G., Ramey Jr., H.J., 1975. Unsteady state pressure distribution created by a directionally drilled well. J. Petrol. Technol. 27 (11), 1392–1400. https://doi.org/10.2118/5131-PA.

Darcy, H., 1856. Les fontaines publiques de la ville de Dijon: exposition et application des principes à suivre et des formules à employer dans les questions de distribution d'eau, vol. 1. Victor dalmont (in French).

Ertekin, T., Abou-Kassem, J.H., King, G.R., 2001. Basic Applied Reservoir Simulation. SPE Textbook Series, New York. https://doi.org/10.2118/9781555630898.

Ezulike, O., Igbokoyi, A., 2012. Horizontal well pressure transient analysis in anisotropic composite reservoirs—a three dimensional semi-analytical approach. J. Petrol. Sci. Eng. 96, 120–139. https://doi.org/10.1016/j.petrol.2012.09.002.

Fair, P.S., Kikani, J., White, C.D., 1999. Modeling high-angle wells in laminated pay reservoirs. SPE Reservoir Eval. Eng. 2 (1), 46–52. https://doi.org/10.2118/54656-PA.

Feng, G.Q., Liu, Q.G., 2015. Pressure transient behavior of a slanted well with an impermeable fault. Journal of Hydrodynamics, Ser. B. 26 (6), 980–985. https://doi.org/10.1016/s1001-6058(14)60108-6.

Gringarten, A.C., Ramey Jr., H.J., 1973. The use of source and green's functions in solving unsteady-flow problems in reservoirs. SPE J. 13 (5), 285–296. https://doi.org/10.2118/3818-PA.

Gill, H., Al-Zayer, R., Issaka, M.B., 2007. Pressure transient behavior of horizontal and slant wells intersecting a high permeability layer. In: SPE Middle East Oil and Gas Show and Conference. https://doi.org/10.2118/105616-MS.

Guan, Z., Chen, T., Liao, H., Guan, Z., Chen, T., Liao, H., 2021. Well trajectory design and wellpath control. Theory and Technology of Drilling Engineering 261–326. https://doi.org/10.1007/978-981-15-9327-7_5.

Holmes, J.A., Barkve, T., Lund, Ø., 1998. Application of a multisegment well model to simulate flow in advanced wells. In: European Petroleum Conference. https://doi.org/10.2118/50646-MS.

Islam, M.R., Hossain, M.E., 2021. Drilling Engineering: towards Achieving Total Sustainability. Gulf Professional Publishing. https://doi.org/10.1016/B978-0-12-820193-0.00008-3.

Khatteb, H.A., Yeh, N.S., Agarwal, R.G., 1991. Pressure transient behavior of slanted wells in single and multiple layered systems. In: SPE Annual Technical Conference and Exhibition. https://doi.org/10.2118/22730-MS.

Luo, W., Tang, C., Feng, Y., 2018. A semianalytical model for horizontal-well productivity with pressure drop along the wellbore. SPE J. 23 (5), 1603–1614. https://doi.org/10.2118/189973-PA.

Miranda, F.A., Barreto Jr., A.B., Peres, A.M., 2016. A novel uniform-flux solution based on the green's function method for modeling the pressure-transient behavior of a restricted-entry well in anisotropic gas reservoirs. SPE J. 21 (5), 1870–1882. https://doi.org/10.2118/180919-PA.

Ozkan, E., Yildiz, T., Raghavan, R., 1999. Pressure transient analysis of perforated slant and horizontal wells. In: SPE Annual Technical Conference and Exhibition. https://doi.org/10.2118/56421-MS.

Ozkan, E., Raghavan, R., 2000. A computationally efficient, transient-pressure solution for inclined wells. SPE Reservoir Eval. Eng. 3 (5), 414–425. https://doi.org/10.2118/66206-PA.

Sousa, B.R., Moreno, R.B., 2015. Transition radial flow in slanted well test analysis. In: SPE Latin American and Caribbean Petroleum Engineering Conference. https://doi.org/10.2118/177034-MS.

Simonov, M.V., Akhmetov, A.V., Roshchektaev, A.P., 2017. Semi-analytical model of transient fluid flow to multilateral well. In: SPE Annual Caspian Technical Conference and Exhibition. https://doi.org/10.2118/189012-MS.

Shi, W., Cheng, J., Liu, Y., Gao, M., Tao, L., Bai, J., Zhu, Q., 2023. Pressure transient analysis of horizontal wells in multibranched fault-karst carbonate reservoirs: model and application in SHB oilfield. J. Petrol. Sci. Eng. 220, 111167. https://doi.org/10.1016/j.petrol.2022.111167.

Teng, B., Li, H.A., 2018. A semi-analytical model for characterizing the pressure transient behavior of finite-conductivity horizontal fractures. Transport Porous Media 123 (2), 367–402. https://doi.org/10.1007/s11242-018-1047-9.

Teng, B., Li, H.A., 2019. Pressure-transient behavior of partially penetrating inclined fractures with a finite conductivity. SPE J. 24 (2), 811–833. https://doi.org/10.2118/194189-PA.

Van Everdingen, A.F., Hurst, W., 1949. The application of the Laplace transformation to flow problems in reservoirs. J. Petrol. Technol. 1 (12), 305–324. https://doi.org/10.2118/949305-g.

Wang, K., Li, Z., Wang, L., Shi, H., Adenutsi, C.D., Wu, J., Wang, C., 2020. A novel semi-analytical model for highly deviated wells in fractured-vuggy carbonate gas reservoirs. In: Offshore Technology Conference Asia. https://doi.org/10.4043/30161-MS.

Xu, Y., Tan, X., Li, X., Li, J., Liu, Q., 2021. Blasingame production decline and production prediction model of inclined well in triple-porosity carbonate gas reservoir. J. Nat. Gas Sci. Eng. 92, 103983. https://doi.org/10.1016/j.jngse.2021.103983.

Zhang, F., Yang, D., 2014. Determination of fracture conductivity in tight formations with non-Darcy flow behavior. SPE J. 19 (1), 34–44. https://doi.org/10.2118/162548-PA.

Zarrouk, S.J., McLean, K., 2019. Advanced analytical pressure-transient analysis relevant to geothermal wells. Geothermal Well Test Analysis 89–111. https://doi.org/10.1016/b978-0-12-814946-1.00005-0.